JARS Journal of Applied Remote Sensing

RESEARCH PAPER

Scientific objectives and instrumental requirements of the infrared spectrometer VenSpec-H onboard EnVision

Séverine Robert,[a,*] Justin T. Erwin,[a] Roderick De Cock,[a] Ian R. Thomas,[a] Nuno Pereira,[a] Lars Jacobs,[a] Sophie Berkenbosch,[a] David Bolsée,[a] Filip Vanhellemont,[a] Eddy Neefs,[a] Shohei Aoki,[b] Bruno Bézard,[c] Emmanuel Marcq,[d] Giulia Alemanno,[e] Joern Helbert,[e] and Ann C. Vandaele[a]

[a]Royal Belgian Institute for Space Aeronomy, BIRA-IASB, Brussels, Belgium
[b]The University of Tokyo, Graduate School of Frontier Sciences, Department of Complexity Science and Engineering, Tokyo, Japan
[c]LESIA, Observatoire de Paris, Université PSL, CNRS, Sorbonne Université, Université de Paris, Meudon, France
[d]LATMOS/IPSL, UVSQ Université Paris-Saclay, Sorbonne Université, CNRS, Guyancourt, France
[e]DLR, Berlin, Germany

ABSTRACT. Onboard the EnVision spacecraft, there will be a suite of three spectrometers, VenSpec. One of these is called VenSpec-H where the H stands for high spectral resolution. Its scientific objectives consist of measuring variations of minor species' abundances in the atmosphere of Venus. H_2O, SO_2, CO, and OCS will be measured to characterize the potentially ongoing volcanic activity. These observations will allow us to understand both the importance of volatiles in volcanic activity on Venus and their effect on cloud maintenance and dynamics. VenSpec-H will measure these molecules in nadir viewing geometry, in infrared transparency windows of Venus' nightside to probe the troposphere, and in infrared spectral ranges on the dayside to measure the mesosphere. The scientific requirements enabling our scientific objectives will be demonstrated. The molecular vertical profiles, the aerosols' model, and the CO_2 continuum contribution were established based on the literature for the different spectral windows. This enabled us to determine the spectral bands, their bandwidth, and the resolving power necessary for our purposes. Along the way, we identified possible improvements and science avenues. Some of them impact the instrument design, such as the need for polarimetric measurements. Others are related to remaining uncertainties in the model and laboratory measurements that will complement the investigation. This has been presented as a poster at the SPIE Optical Engineering + Applications Conference in August 2024 in San Diego, California, United States.

Keywords: EnVision; VenSpec-H; radiative transfer theory; Venus; molecular species; volcanic activity; instrumental requirements

Paper 240631G received Oct. 16, 2024; revised Feb. 13, 2025; accepted Mar. 10, 2025; published Mar. 31, 2025.

*Address all correspondence Séverine Robert, severine.robert@aeronomie.be

Handling Editor: Shen-En Qian, Associate Editor

1 Introduction

Despite their similar size and bulk composition, Venus and Earth have followed different geological evolution paths. In 2 years of radar mapping (1990 to 1992), Magellan showed that Venus has abundant volcanic and tectonic features but was unable to detect ongoing geological activity.[2] Hahn and Byrne[3] published a global catalog of volcanoes describing around 85,000 edifices, ~99% of which are less than 5 km in diameter. They noticed a lack of edifices in the 20 to 100 km diameter range. In 2005, Venus Express was launched with a payload focusing on atmospheric science. The scientific phase of the mission (2006 to 2014) was a success and provided hints of active volcanism. More specifically, three instruments onboard Venus Express brought insights to this investigation. First, the Visible and Infrared Thermal Imaging Spectrometer (VIRTIS) detected local anomalies in the emissivity maps.[4] The infrared radiation coming from three volcanic regions was different to that from the surrounding terrain and interpreted as coming from relatively fresh lava flows that had not yet experienced significant surface weathering. Although these flows were found to be less than 2.5 million years old, the study could not establish whether there is still active volcanism on the planet. Second, the "Spectroscopy for Investigation of Characteristics of the Atmosphere of Venus" (SPICAV)-UV channel was used to measure the abundances of SO_2 above the cloud level.[5] Complementing the series of measurements done by UVIS onboard Pioneer Venus during the 1970s and 1980s,[6–8] the SPICAV-UV measurements showed a sharp rise in the sulfur dioxide content of the upper atmosphere in 2006 to 2007, followed by a gradual fall over the following 5 years.[9] As suggested by Marcq et al., these episodic sulfur dioxide injections to the cloud tops may be caused either by periods of increased buoyancy of volcanic plumes or, in the absence of active volcanism, by long-period oscillations of the general atmospheric circulation. Finally, another striking evidence for active volcanism on Venus came from the Venus Monitoring Camera (VMC) in 2014. VMC spotted localized changes in the surface brightness among images taken only a few days apart in 2008 and 2009. These infrared "flashes" over the edges of the rift zone Ganis Chasma are thought to be caused either by hot gases and/or lava released from volcanic eruptions.[10] Since Venus Express, more investigations have been carried out, and recently, Herrick and Hensley[11] and Sulcanese et al.[12] identified evidences of ongoing volcanic activities using the Magellan dataset.

To determine whether Venus is geologically active, a comprehensive payload is necessary: the surface and subsurface need to characterized, but information about the atmosphere is crucial. This is why EnVision will also carry a complete spectroscopy suite called VenSpec[13] including an infrared mapper, VenSpec-M;[14] an ultraviolet spectrometer, VenSpec-U;[15] and an infrared spectrometer, VenSpec-H.[16]

2 Scientific Objectives and Requirements

The science objectives of the VenSpec suite are to search for temporal variations in surface temperatures and tropospheric concentrations of volcanically emitted gases, indicative of volcanic eruptions; to study surface-atmosphere interactions and weathering by mapping surface emissivity and tropospheric gas abundances; and to map the variability of trace species, cloud, and aerosol properties and to distinguish intrinsic from extrinsic (e.g., volcanic emissions) variabilities in the mesosphere. Observations will provide insight into the spatial distribution of trace gas which is essential to understand the main chemical cycles on Venus. Any photon that is emitted from the surface will encounter multiple scattering at particles in the clouds in a way that results in a blurring of the images. Models have predicted a limit of the spatial resolution of 50 to 100 km.[17,18] This was confirmed by analysis of the VIRTIS dataset early during the Venus Express mission.[19]

Observing Venus' troposphere in the infrared is challenging. On the dayside of the planet, the reflected sunlight on the cloud deck prevents measuring below the clouds. The nightside of the planet must then be targeted. Straylight from the dayside and high density of CO_2 rendering the atmosphere opaque limit the number of useful spectral ranges. Molecular species are probed in specific spectral windows called transparency windows centered at 1.0, 1.1, 1.2, 1.3, 1.7, and 2.3 μm.[20] They have been used extensively since the 1990s to retrieve SO_2, OCS, CO, H_2O, and HCl[21–27] in the lower layers of the atmosphere, but so far, only vertical profiles of the H_2O could be determined.

R2-C-10 (Sect. 3.5.1)	Map **tropospheric gases** at **0-45 km altitude**: (1) H_2O partial column random error: < 10% (and < 20% below 15 km altitude) (2) HDO partial column random error: < 20% (and < 30% below 15 km altitude) (3) CO partial column random error: < 14% (4) OCS partial column random error: < 18% (5) SO_2 partial column random error: < 30% at a **horizontal resolution of < 100 km (and < 200 km for H_2O and HDO below 15 km altitude)**, to detect gradients related to surface-atmosphere and cloud interaction processes.
R2-C-20 (Sect. 3.5.3)	Map **mesospheric gases** at **65-80 km altitude**: (1) SO_2 partial column random error: < 20% (2) SO:SO_2 partial column random error: < 25% at a **spatial resolution of 5 (small-scale convection and vertical mixing) to 50 km at UV wavelength** (3) H_2O partial column random error: < 20% (4) HDO partial column random error: < 20% (5) H_2O:HDO partial column random error: < 25% (6) SO_2 partial column random error: < 20% (7) CO partial column random error: < 20% (8) OCS partial column random error: < 20% at a **spatial resolution of <50 km at IR wavelength** in order to assess coupling between surface (volcanic activity, topographic features), cloud and mesospheric measurements.

Fig. 1 EnVision Science observation requirements summary extracted from the Red Book.[31] "In the left-hand column, the EnVision requirements number is noted, together with a reference to the sections describing further the requirement flow-down and how the science objectives are met applying the intended observation strategy and mission payloads." The requirement R2-C-20 (2) is associated to VenSpec-U.[15,32,33]

The dayside measurements provide information about the mesosphere. In synergy with VenSpec-U, the possible exchange occurring between the layers below and above the clouds will be investigated, especially in the case of the detection of a plume. In preparation for the mission, the potential impacts of a volcanic plume have been discussed,[28] and modeling efforts are ongoing.[29,30]

Based on our knowledge so far, the science requirements for the mission were decided upon and those related to VenSpec-H are summarized in Fig. 1.

Simultaneous observations of different species at a high spectral resolution will be the asset of our VenSpec-H experiment. Few investigations reported measurements of different molecular species in the same spectra. Nevertheless, anti-correlation was highlighted between SO_2 and H_2O[34] or OCS and CO.[26] The new instrumentation will enable us to derive a map of these four molecular species altogether. This will be done by measuring a wide spectral range in the 2.3 μm window at high spectral resolution. As will be discussed, the bandwidth is limited by the spectral resolution that needs to be as high as possible to be able to differentiate the ro-vibrational lines for each molecule. This requirement will be translated into an increase of the resolving power by a factor of 4 to 5 compared with VIRTIS-H/Venus Express ($R = 2000$). A higher spectral resolution has already proven being decisive in highlighting variation of SO_2 in the 2.46 μm band.[35] Using radiative transfer tools and our expertise with the NOMAD-LNO instrument onboard ExoMars Trace Gas Orbiter,[36] we describe the instrumental requirements of this new experiment capable of measuring trace gases at high resolution both in the troposphere and in the mesosphere of the Venus atmosphere.

3 Modeling the Venus Atmosphere

3.1 Radiative Transfer Code

To define the instrumental requirements of a new experiment, such as the signal-to-noise ratio (SNR), the resolving power (RP), and the spectral ranges, our radiative transfer code ASIMUT-ALVL was used extensively. ASIMUT is a modular program for radiative transfer calculations in planetary atmospheres.[37] One of the main particularities of the software is the possibility to retrieve columns and/or profiles of atmospheric constituents simultaneously from different spectra, which may have been recorded by different instruments or obtained under different geometries. This allows the possibility to perform combined retrieval, e.g., of a ground-based measurement and a satellite-based one probing the same air mass or from spectra recorded by different instruments on the same platform.[38] This radiative transfer code derives the Jacobians analytically and includes the optimal estimation method,[39] using diagonal or full covariance matrices.

Initially developed for the Earth's atmosphere, its applicability has been extended to extra-terrestrial atmospheres, such as those of Mars[40–42] and Venus.[43] ASIMUT has been coupled to SPHER/TMATRIX[44,45] and LIDORT[46] codes to include the complete treatment of the scattering effects in the radiative transfer calculations.[47]

ASIMUT-ALVL can be used as a forward modeling tool and also as a retrieval module. It allows to fit simultaneously or sequentially different parts of one or more spectra, to fit the surface temperature, to fit column/vertical profiles for molecular species and for aerosols, and to fully characterize the outputs (averaging kernels, errors, degrees of freedom, etc.).

3.2 Molecular Data

When simulating the Venus atmosphere in the infrared spectral ranges, eight molecular species are needed: CO_2, H_2O, HDO, CO, SO_2, HCl, HF, and OCS. Each of them has their own absorption spectrum. Figure 2 shows the line intensities directly downloaded from HITRAN Online.[76] It shows how interesting the 2.3 to 2.5 μm spectral range is. The CO band is visible at one end and the SO_2 one at the other. HF lines are more spaced to one another, due to the rotational constant of the molecule. In terms of intensity, the SO_2 band is weak compared with the rest.

The line parameters were extracted from the HITRAN Online database[48] using HAPI.[77] The broadening line parameters have not been modified accounting for the CO_2 buffer atmosphere. This was a deliberate choice as in the frame of this investigation, our model still needed to be validated. Line parameters associated with a CO_2 atmosphere are available in the literature for some spectral regions[78–81] and will be taken into account in further works.[82] This choice is supported by the fact that only simulations were done and the impact of one set of line parameters over the other is low. In the next phase of the mission preparation, when retrievals are performed, adequate parameters will need to be used as the retrieved abundances are affected by this choice.[83–85] HITEMP2010[86] and HITRAN Online for H_2O were both considered for this investigation. The spectroscopic databases and their different versions are regularly the topics of validation papers[87–89] as none is perfect. We decided to use the most recent one at a standard temperature for traceability reasons first and also because the conclusion reached with this line list should still hold with a more complete line list, more consistent for the high temperature of the Venus atmosphere.

The vertical profiles of the different molecules are shown in Fig. 3.

The high pressure of the Venus' troposphere leads to collisional effects on molecular spectra.[98] No theoretical model is perfect yet, and *ad hoc* solutions are used. Especially, two important effects of pressure were mitigated in our radiative transfer model. First, to account for the far wings, each of the absorption lines is calculated on a 250-cm^{-1} spectral interval, i.e., 125 cm^{-1} on each side of the line center. A Voigt profile was used for all molecules except for CO_2 which requires a sublorentzian profile.[99] Second, the CO_2 continuum was prescribed

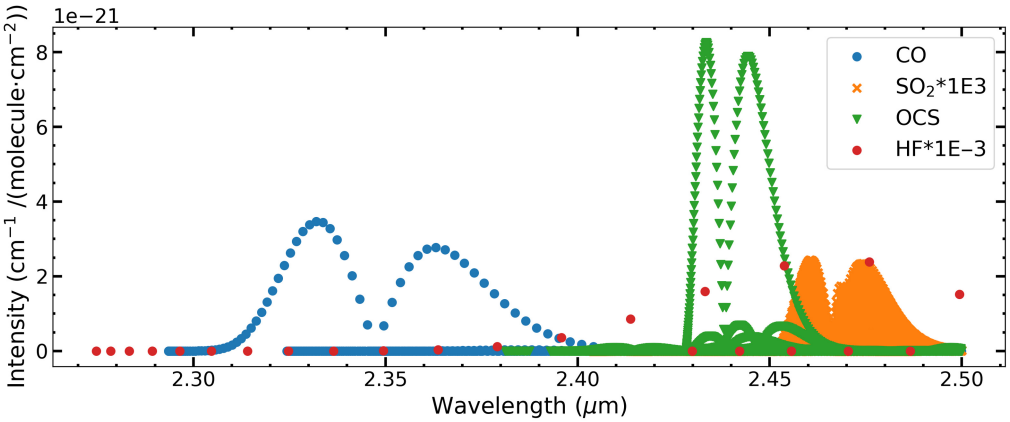

Fig. 2 Line intensities of CO in blue, SO_2 in orange with a multiplicative factor of 10^3, OCS in green, and HF in red with a multiplicative factor of 10^{-3}. The values have been downloaded from HITRAN Online on July 24, 2024.[48–75] Water lines are not shown for better readability, but they do absorb in that spectral range.

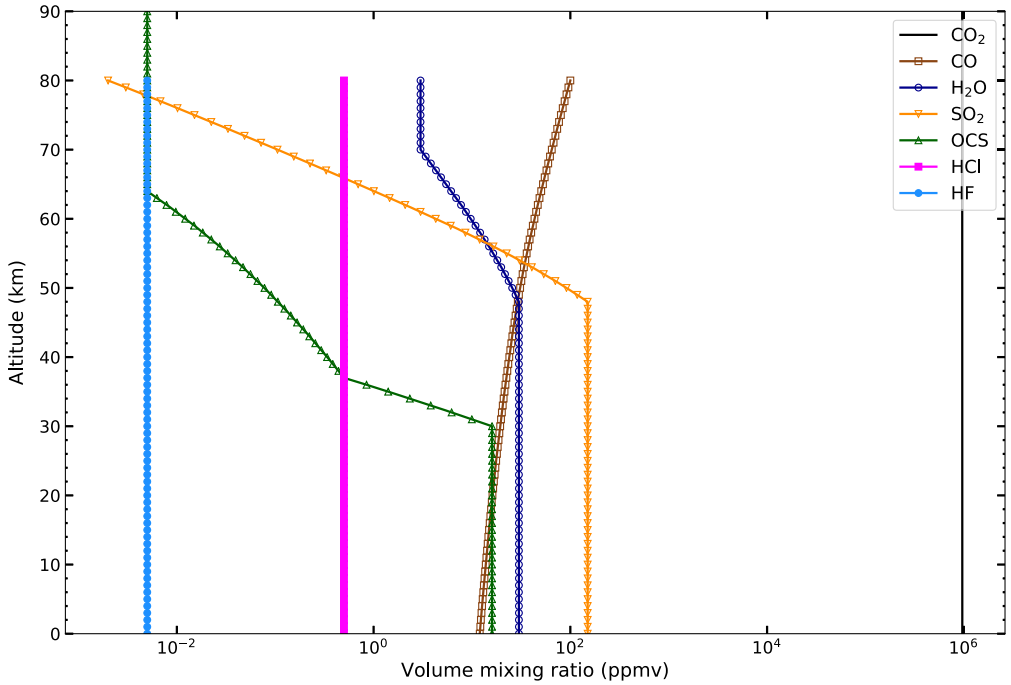

Fig. 3 Molecular species profiles used in this work.[90–97]

based on the same methodology as in Refs. 99–102. Empirical values based on the VIRTIS/Venus Express spectra were determined and used.

3.3 Atmospheric Data

ASIMUT-ALVL was used to calculate synthetic spectra, using a line-by-line approach. Simulations of the dayside and the nightside of the Venus atmosphere were performed in the infrared spectral region spanning wavelengths from 1 to 2.6 μm. Eight molecular species were

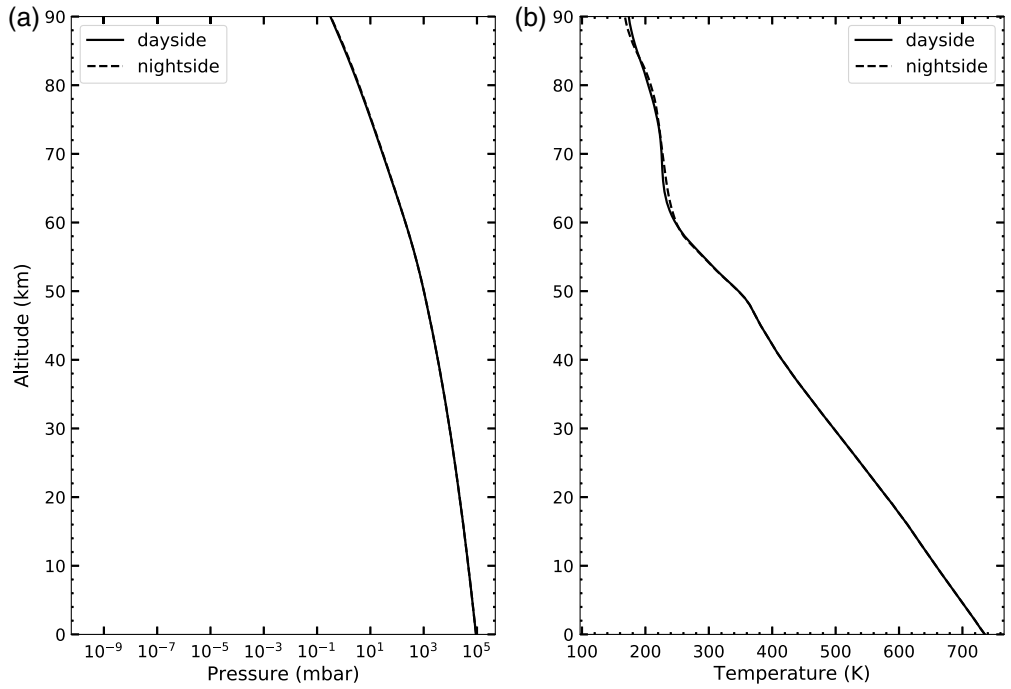

Fig. 4 Pressure (a) in log scale and temperature (b) profiles in function of altitude, used in this work.[91,95]

Table 1 Mean radius and variance of the different modes of the Venus' aerosols.

Mode	mean radius [μm]	σ [–]
1	0.3	1.56
2	1.0	1.29
2p	1.4	1.23
3	3.65	1.28

included, CO_2, H_2O, HDO, CO, SO_2, HCl, HF, and OCS, as well as the aerosols and the CO_2 continuum contribution. The concentration profiles of the molecular species are based on the literature[90–94,103] and further refined into a common reference scenario defined at the mission level. Rayleigh scattering was also taken into account.[104]

The temperature and pressure profiles were obtained from the literature,[91,95] as shown in Fig. 4.

The description of the cloud layer was based on former studies, namely, Refs. 101 and 105. Because the particles are liquid and approximately spherical, and because the wavelength of the light is of the same order as the radius of the particles, a Mie code is appropriate for the calculation of their scattering properties. The particle number densities of four cloud modes were distributed from 0 to 100 km according to Figure 12 in Ref. 101. The modes themselves are described in Table 1. We assumed a lognormal distribution of sizes and the refractive indices were taken from Ref. 106.

4 Instrumental Requirements

Based on the quantities described in Sec. 3, spectral simulations were performed. The radiance of the nightside comes from the thermal emission of the surface and atmosphere, whereas on the dayside, where we considered a solar zenith angle of 30 deg, there is an additional solar reflectance contribution. We used our tool to determine the following:

- limits of the spectral ranges and the resolving power
- signal-to-noise ratio.

4.1 Bandwidth and Resolving Power

The baseline of our instrument is based on SOIR/Venus Express[43,107] and NOMAD-LNO/ExoMars Trace Gas Orbiter.[108,109] To retain much heritage from these successful instruments, the optical concept of our VenSpec-H spectrometer is based on an echelle grating coupled to a high-performance, actively cooled detector.[16] The characteristics of the echelle grating that define the free spectral range and the instrument line profile and of the detector, i.e., its size in pixels, need to be taken into account when defining the scientific requirements. Bandwidth and spectral resolution must be balanced out. The resolving power of a grating spectrometer with well-corrected optics is independent of the wavelength. It defines the smallest difference in wavelength of two spectral lines that can be distinguished from one another. The bandwidth is the wavelength range seen by the detector. They are defined by the following Eq. (1):

$$R_{\max} = \frac{n_{\text{pix}} \times 10000}{\lambda \times \text{BW}} \tag{1}$$

where $R_{\max}$ is the maximum resolving power, n_{pix} is the number of pixels in the spectral direction, and BW is the bandwidth.

As an example, let us imagine a detector of 500 pixels wide, in the spectral direction. To achieve a resolving power of 7000 in the 2.5-μm band, Eq. (1) indicates that the bandwidth cannot be larger than 285.7 cm^{-1}. Besides, the minimum value of bandwidth assumes that the pixel pitch is the limiting factor and that the full width at half maximum of the instrumental line profile, i.e., the image of the slit for monochromatic illumination, is not wider than one pixel.

If a slit is used with an equivalent width of more than one pixel, the maximum bandwidth is divided by the slit width in pixels. In other words, the higher the resolving power, the narrower the bandwidth for a fixed number of pixels.

A trade-off must be found here. On one hand, measuring simultaneously CO and SO_2, so far apart in wavelength, as shown in Fig. 2 imposes a bandwidth of several hundreds of wavenumbers. On the other hand, a high resolving power is required to distinguish the spectral features of H_2O in the 1.17-μm band, as shown in Fig. 5. This led to strong constraints on the optical design.[16,110]

The physical characteristics of the grating may deviate from the ideal band centers when deriving them only based on spectroscopy. One band center may be selected very precisely. The other wavelength ranges probed will flow down from this first choice. Considering the scientific objectives of the mission and of the instrument, the cold overtone vibrational band $3\nu_3$ (003-000) of SO_2, centered at 2.45 μm, is considered as the primary target, and the optical design was optimized accordingly.

4.2 Signal-to-Noise Ratio

To determine the required SNR, radiances were simulated at two resolving powers (RP = 7000 and 8500), and noise was added before performing the retrievals with ASIMUT-ALVL. The science objective of 10% accuracy on each molecule was the target (except in the spectral band probing the near-surface contents), see Fig. 1.

The error budget on the retrieved abundances was estimated considering the following contributions:

- random error: retrieval error directly from the fit
- systematic errors: cross-sections (3%), raytracing (1%), and source term (night: 1.2%; day: 3.6%).

The considered systematic errors are originating from unavoidable uncertainties in the radiative transfer model. The uncertainties on the cross sections are linked to the choice of spectroscopy (HITEMP and HITRAN, with or without CO_2 broadening). All line parameters are not available yet for Venus' conditions. Besides the error on intensities, for instance, H_2O varies from HITRAN error level 8 to 3, i.e., from less than 1% to above 20% relative error. The other molecules errors are mostly around 5% to 10% on their line intensities. In our error budget,

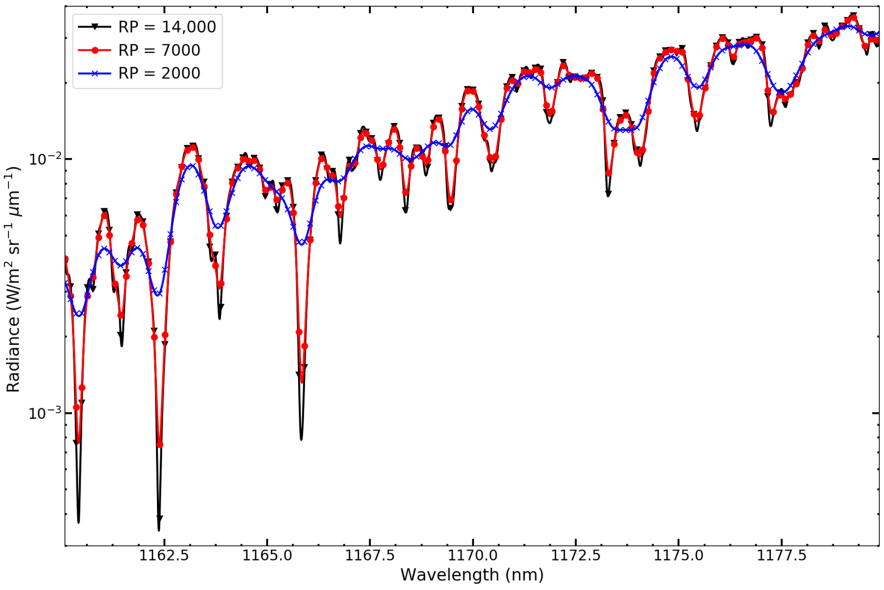

Fig. 5 Simulated radiance of the Venus atmosphere at different resolving powers: 14,000 in black, 7000 in red, and 2000 in blue. To distinguish among the different spectral lines, a resolving power of at least 7000 is required.

we assumed a 3% error on the calculated cross-sections based on these HITRAN parameters. The raytracing error is defined based on what impact could a pointing error have in the optical path length. The source term errors on the nightside were calculated based on the impact on the Planck function when varying the surface temperature by 1 K. For the dayside, a factor of 3 was added to this error to take into account the complexity of the incoming radiation.

The error budget in % was plotted against the SNR values, as shown in Fig. 6. The SNR value to meet the required accuracy was obtained by interpolation as shown by the dotted lines in Fig. 6. This was done for each molecule in each spectral band (B).

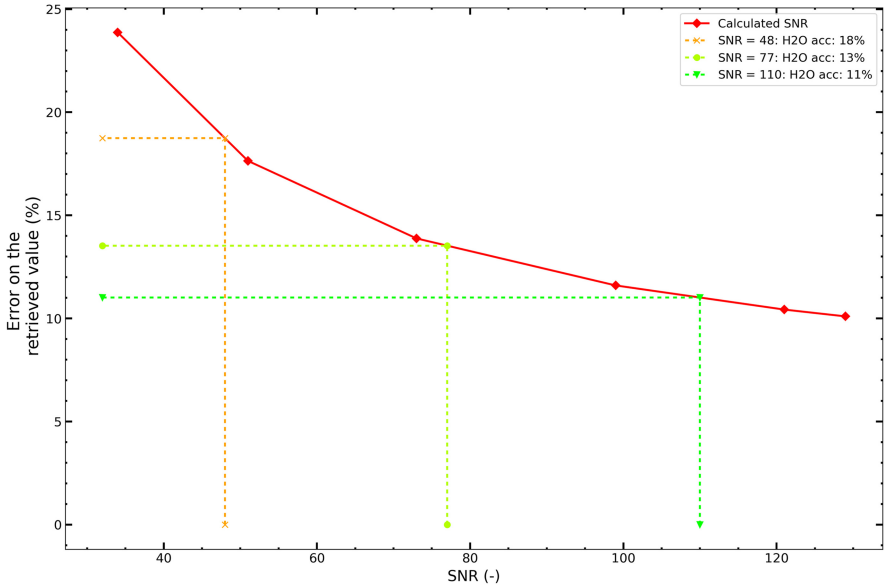

Fig. 6 Error budget of Band1 (B1) on the nightside for H_2O. As expected, the accuracy depends on the achievable SNR.

Table 2 Spectral bands, as defined after this investigation. The required resolving power is 7000.

	Band limits (nm)	Band limits (cm^{-1})	Bandwidth (cm^{-1})	Required SNR	Molecular species	Altitude range (km)
Nightside						
B1	1160 to 1180	8474 to 8621	147	48	H_2O and HDO	0 to 15 km
B2a	2340 to 2420	4132 to 4274	142	126	CO, H_2O, HDO, OCS, and HF	30 to 45 km
B2b	2423 to 2507	3989 to 4127	138	126	SO_2, H_2O, HDO, OCS, and HF	30 to 45 km
B3	1704 to 1747	5724 to 5868	144	70	H_2O and HCl	20 to 30 km
Dayside						
B2a	2340 to 2420	4132 to 4274	142	100	CO, H_2O, HDO, OCS, and HF	55 to 80 km
B2b	2423 to 2507	3989 to 4127	138	100	SO_2, H_2O, HDO, OCS, and HF	55 to 80 km
B4	1367 to 1394	7174 to 7315	141	100	H_2O and HDO	55 to 80 km

5 Conclusions

In this investigation, the molecular vertical profiles, the aerosols' model, and the CO_2 continuum contribution were validated for the different spectral windows. This enabled us to determine the spectral bands, their bandwidth, and the resolving power necessary for our purposes. These values were confirmed as acceptable by performing retrievals for each spectral band. Diagnostics tools, such as the residuals of the fit and the degree of freedom for each species, were analyzed. The science requirements are driven by the lowest resolving power enabling the detection and the retrieval of the abundance of the different molecular species. The resolving power versus bandwidth trade-off has been investigated bearing in mind instrumental capabilities to reach a sensible solution, allowing us to resolve ro-vibrational lines with a high spectral resolution and cover as wide as possible spectral range to measure simultaneously different molecular trace gases.

Table 2 summarizes the results obtained in this investigation.

In the near future, we will strengthen our model by comparing it to previous datasets from VIRTIS/Venus Express.[102,111] Possible improvements are related to remaining uncertainties in the model such as for the CO_2 continuum treatment. A campaign of laboratory measurements that will complement the investigation has started[82] and will continue. New science avenues impacted the design, such as the need for polarimetric measurements.[112]

Disclosures

The authors declare that there are no financial interests, commercial affiliations, or other potential conflicts of interest that could have influenced the objectivity of this research or the writing of this paper.

Code and Data Availability

The ASIMUT-ALVL code is made of two main components: ASIMUT which is an in-house radiative transfer model, available on demand to the BIRA-IASB team, and LIDORT which is developed by R. Spurr and available for download on http://rtslidort.com

The data for the molecular absorption are available on HITRAN (https://hitran.org/). The atmospheric scenario, including the aerosols' distribution, is described in sufficient detail in the paper and is based on a literature review.

Acknowledgments

This work has been performed with the support of the Belgian Science Policy Office (Contract No. 4000144206), with financial and contractual coordination by the ESA Prodex Office. EM acknowledges the support from CNES and ESA for all EnVision-related activities.

References

2. J. W. Head et al., "Venus initial analysis from Magellan data," *Science* **252**, 276–288 (1991).
3. R. Hahn and P. Byrne, "A morphological and spatial analysis of volcanoes on Venus," *J. Geophys. Res. Planets* **128**, e2023JE007753 (2023).
4. S. E. Smrekar et al., "Recent hotspot volcanism on Venus from VIRTIS emissivity data," *Science* **328**, 605–608 (2010).
5. E. Marcq et al., "Variations of sulphur dioxide at the cloud top of Venus' dynamic atmosphere," *Nat. Geosci.* **6**, 25–28 (2013).
6. L. W. Esposito, J. R. Winick, and A. I. Stewart, "Sulfur dioxide in the Venus atmosphere—distribution and implications," *Geophys. Res. Lett.* **6**, 601–604 (1979).
7. L. W. Esposito, "Sulfur dioxide—episodic injection shows evidence for active Venus volcanism," *Science* **223**, 1072–1074 (1984).
8. L. W. Esposito et al., "Sulfur dioxide at the Venus cloud tops, 1978-1986," *J. Geophys. Res.* **93**, 5267–5276 (1988).
9. E. Marcq et al., "Climatology of SO_2 and UV absorber at Venus' cloud top from SPICAV-UV nadir dataset," *Icarus* **335**, 113368 (2020).
10. E. V. Shalygin et al., "Active volcanism on Venus in the Ganiki Chasma rift zone," *Geophys. Res. Lett.* **42**, 4762–4769 (2015).

11. R. R. Herrick and S. Hensley, "Surface changes observed on a Venusian volcano during the Magellan mission," *Science* **379**, 1205–1208 (2023).
12. D. Sulcanese, G. Mitri, and M. Mastrogiuseppe, "Evidence of ongoing volcanic activity on Venus revealed by Magellan radar," *Nat. Astron* **8**, 973–982 (2024).
13. J. Helbert et al., "The VenSpec suite on the ESA EnVision mission to Venus," *Proc. SPIE* **11128**, 1112804 (2019).
14. J. Helbert et al., "The Venus Emissivity Mapper (VEM): obtaining global mineralogy of Venus from orbit," *Proc. SPIE* **10765**, 107650D (2018).
15. E. Marcq et al., "Instrumental requirements for the study of Venus' cloud top using the UV imaging spectrometer VeSUV," *Adv. Space Res.* **68**(1), 275–291 (2021).
16. E. Neefs et al., "VenSpec-H spectrometer on the ESA EnVision mission: design, modeling and analysis," *Acta Astronaut.* **226**(1), 178–201 (2025).
17. G. Hashimoto and S. Sugita, "On observing the compositional variability of the surface of Venus using nightside near-infrared thermal radiation," *J. Geophys. Res.* **108**(E9), 5109 (2003).
18. V. Moroz, "Estimates of visibility of the surface of Venus from descent probes and balloons," *Planet. Space Sci.* **50**, 287–297 (2002).
19. J. Helbert et al., "Surface brightness variations seen by VIRTIS on Venus Express and implications for the evolution of the Lada Terra region, Venus," *Geophys. Res. Lett.* **35**, L11201 (2008).
20. R. W. Carlson et al., "Galileo infrared imaging spectroscopy measurements at Venus," *Science* **253**, 1541–1548 (1991).
21. B. Bézard and C. de Bergh, "Composition of the atmosphere of Venus below the clouds," *J. Geophys. Res.* **112**, E04S07 (2007).
22. C. C. C. Tsang et al., "Tropospheric carbon monoxide concentrations and variability on Venus from Venus Express/VIRTIS-M observations," *J. Geophys. Res.* **113**, E00B08 (2008).
23. N. Iwagami et al., "Hemispheric distributions of HCl above and below the Venus' clouds by ground-based 1.7 μm spectroscopy," *Planet. Space Sci.* **56**, 1424–1434 (2008).
24. N. Iwagami et al., "Hemispherical distribution of CO above the Venus' clouds by ground-based 2.3 μm spectroscopy," *Icarus* **207**, 558–563 (2010).
25. E. Marcq et al., "A latitudinal survey of CO, OCS, H_2O, and SO_2 in the lower atmosphere of Venus: spectroscopic studies using VIRTIS-H," *J. Geophys. Res.* **113**, E00B07 (2008).
26. G. Arney et al., "Spatially resolved measurements of H_2O, HCl, CO, OCS, SO_2, cloud opacity, and acid concentration in the Venus near-infrared spectral windows," *J. Geophys. Res. Planets* **119**, 1860–1891 (2014).
27. E. Marcq et al., "Minor species in Venus' night side troposphere as observed by VIRTIS-H/Venus Express," *Icarus* **405**, 115714 (2023).
28. C. F. Wilson et al., "Possible effects of volcanic eruptions on the modern atmosphere of Venus," *Space Sci. Rev.* **220**, 31 (2024).
29. M. Lefèvre, E. Marcq, and F. Lefèvre, "The impact of turbulent vertical mixing in the Venus clouds on chemical tracers," *Icarus* **386**, 115148 (2022).
30. M. Lefèvre, "Venus boundary layer dynamics: Eolian transport and convective vortex," *Icarus* **387**, 115167 (2022).
31. A. Straume et al., "Envision definition study report," tech. rep., ESA, https://www.cosmos.esa.int/documents/10892653/0/EnVision+Red+Book_ESA-SCI-DIR-RP-003+(1).pdf/b037b151-f4fe-303a-f6c6-430c605a407f?t=1706621315626 (2023).
32. L. Conan et al., "The VenSpec-U spectrometer onboard EnVision mission: a sensitivity study," *Proc. SPIE* **13144**, 131440L (2024).
33. B. Lustrement et al., "Design of the VenSpec-U instrument on board EnVision," *Proc. SPIE* **13144**, 13144–20 (2024).
34. T. Encrenaz et al., "HDO and SO_2 thermal mapping on Venus. IV. Statistical analysis of the SO_2 plumes," *Astron. Astrophys.* **623**, A70 (2019).
35. E. Marcq et al., "Evidence for SO_2 latitudinal variations below the clouds of Venus," *AA* **648**, L8 (2021).
36. S. Robert et al., "Expected performances of the NOMAD/ExoMars instrument," *Planet. Space Sci.* **124**, 94–104 (2016).
37. A. C. Vandaele, M. Kruglanski, and M. De Mazière, "Modeling and retrieval of atmospheric spectra using ASIMUT," in *Proc. First Atmos. Sci. Conf., ESRIN*, Frascati (2006).
38. S. Robert et al., "Two test-cases for synergistic detections in the Martian atmosphere: carbon monoxide and methane," *J. Quant. Spectrosc. Radiat. Transf.* **189**, 86–104 (2017).
39. C. D. Rodgers, *Inverse Methods for Atmospheric Sounding—Theory and Practice*, Atmospheric Oceanic and Planetary Physics, Vol. **2** (2000).
40. R. Drummond et al., "Studying methane and other trace species in the Mars atmosphere using a SOIR instrument," *Planet. Space Sci.* **59**, 292–298 (2011).

41. S. Aoki et al., "Annual appearance of hydrogen chloride on Mars and a striking similarity with the water vapor vertical distribution observed by TGO/NOMAD," *Geophys. Res. Lett.* **48**(11), e2021GL092506 (2021).
42. L. Trompet et al., "Carbon dioxide retrievals from NOMAD-SO on ESA's ExoMars trace gas orbiter and temperature profiles retrievals with the hydrostatic equilibrium equation: 1. Description of the method," *J. Geophys. Res. Planets* **128**(3), e2022JE007277 (2023).
43. A. C. Vandaele et al., "Composition of the Venus mesosphere measured by solar occultation at infrared on board Venus Express," *J. Geophys. Res. (Planets)* **113**, E00B23 (2008).
44. M. I. Mischenko and L. D. Travis, "Capabilities and limitations of a current Fortran implementation of the T-matrix method for randomly oriented, rotationally symmetric scatterers," *J. Quant. Spectrosc. Radiat. Transf.* **60**, 309–324 (1998).
45. M. I. Mishchenko et al., "Comprehensive T-matrix reference database: a 2007–2009 update," *J. Quant. Spectrosc. Radiat. Transf.* **111**, 650–658 (2010).
46. R. J. D. Spurr, T. P. Kurosu, and K. V. Chance, "A linearized discrete ordinate radiative transfer model for atmospheric remote-sensing retrieval," *J. Quant. Spectrosc. Radiat. Transf.* **68**, 689–735 (2001).
47. S. Vandenbussche et al., "Retrieval of desert dust aerosol vertical profiles from IASI measurements in the TIR atmospheric window," *Atmos. Meas. Tech.* **6**, 2577–2591 (2013).
48. I. E. Gordon et al., "The HITRAN2020 molecular spectroscopic database," *J. Quant. Spectrosc. Radiat. Transf.* **277**, 107949 (2022).
49. R. Hashemi et al., "Improvement of the spectroscopic parameters of the air- and self-broadened N_2O and CO lines for the HITRAN2020 database applications," *J. Quant. Spectrosc. Radiat. Transf.* **271**, 107735 (2021).
50. V. M. Devi et al., "Spectral line parameters including temperature dependences of air-broadening for the 2→0 bands of $^{13}C^{16}O$ and $^{12}C^{18}O$ at 2.3 μm," *J. Mol. Spectrosc.* **276-277**, 33–48 (2012).
51. C. Pollock et al., "Absolute frequency measurements of the 2-0 band of CO at 2.3 μm; calibration standard frequencies from high resolution color center laser spectroscopy," *J. Mol. Spectrosc.* **99**, 357–368 (1983).
52. G. Li et al., "Rovibrational line lists for nine isotopologues of the CO molecule in the X^1sigma^+ ground electronic state," *Astrophys. J. Suppl. Ser.* **216**, 15 (2015).
53. L. Rothman et al., "The HITRAN 2004 molecular spectroscopic database," *J. Quant. Spectrosc. Radiat. Transf.* **96**, 139–204 (2005).
54. V. M. Devi et al., "Spectral line parameters including temperature dependences of self- and air-broadening in the 2→0 band of CO at 2.3 μm," *J. Quant. Spectrosc. Radiat. Transf.* **113**, 1013–1033 (2012).
55. V. M. Devi et al., "Erratum to "Spectral line parameters including temperature dependences of self- and air-broadening in the 2→0 band of CO at 2.3 μm"," *J. Quant. Spectrosc. Radiat. Transf.* **116**, 199–200 (2013).
56. J. A. Coxon and P. Hajigeorgiou, "Direct potential fit analysis of the $X^1\sum^+$ ground state of CO," *J Chem Phys* **121**, 2992–3008 (2004).
57. Y. Tan et al., *The Broadening Coefficients of SO_2*, Zenodo (2016).
58. N. Tasinato et al., "A complete listing of sulfur dioxide self-broadening coefficients for atmospheric applications by coupling infrared and microwave spectroscopy to semiclassical calculations," *J. Quant. Spectrosc. Radiat. Transf.* **130**, 233–248 (2013).
59. O. V. Naumenko and V.-M. Horneman, "$^{32}S^{16}O_2$ line list," Private communication (2019).
60. D. S. Underwood et al., "ExoMol molecular line lists—XIV. The rotation-vibration spectrum of hot SO_2," *Mon. Not. R. Astron. Soc.* **459**, 3890–3899 (2016).
61. J. L. Domenech, D. Bermejo, and J. P. Bouanich, "Pressure lineshift and broadening coefficients in the $2\nu_3$ band of OCS," *J. Mol. Spectrosc.* **200**, 266–276 (2000).
62. M. Koshelev and M. Tretyakov, "Collisional broadening and shifting of OCS rotational spectrum lines," *J. Quant. Spectrosc. Radiat. Transf.* **110**, 118–128 (2009).
63. J.-P. Bouanich et al., "Diode laser measurements of line strengths and collisional halfwidths in the ν_1 band of OCS at 298 K and 200 K," *J. Quant. Spectrosc. Radiat. Transf.* **36**, 295–306 (1986).
64. K. Sung et al., "Line strength measurements of carbonyl sulfide $^{16}O^{12}C^{32}S$ in the $2\nu_3$, $\nu_1+2\nu_2+\nu_3$, and $4\nu_2+\nu_3$ bands," *J. Quant. Spectrosc. Radiat. Transf.* **110**, 2082–2101 (2009).
65. R. Toth et al., "Line positions and strengths of 41 bands including 10 OCS isotopologues in the 3850-4200 cm^{-1}," *J. Quant. Spectrosc. Radiat. Transf.* **111**, 1193–1208 (2010).
66. S. Naïm et al., "Fourier transform spectroscopy of carbonyl sulfide from 3700 to 4800 cm^{-1} and selection of a line-pointing program," *J. Mol. Spectrosc.* **192**, 91–101 (1998).
67. A. Pine and J. Looney, "N_2 and air broadening in the fundamental bands of HF and HCl," *J. Mol. Spectrosc.* **122**, 41–55 (1987).
68. G. Guelachvili and M. Smith, "Measurements of pressure-induced shifts in the 1-0 and 2-0 bands of HF and in the 2-0 bands of $H^{35}CI$ and $H^{37}CI$," *J. Quant. Spectrosc. Radiat. Transf.* **20**, 35–47 (1978).
69. A. Pine and A. Fried, "Self-broadening in the fundamental bands of HF and HCl," *J. Mol. Spectrosc.* **114**, 148–162 (1985).

70. J. Coxon and P. Hajigeorgiou, "Breakdown of the Born-Oppenheimer approximation in the ground electronic state of hydrogen halides: improved direct potential fitting analyses for HF/DF/TF, HCl/DCl/TCl, HBr/DBr/TBr and HI/DI/TI," *J. Quant. Spectrosc. Radiat. Transf.* **151**, 133–154 (2015).
71. G. Li et al., "Reference spectroscopic data for hydrogen halides. Part I: Construction and validation of the ro-vibrational dipole moment functions," *J. Quant. Spectrosc. Radiat. Transf.* **121**, 78–90 (2013).
72. R. Meredith and F. Smith, "Broadening of hydrogen fluoride lines by H_2, D_2, and N_2," *J Chem Phys* **60**, 3388–3391 (1974).
73. S.-I. Chou, D. Baer, and R. Hanson, "Diode-laser measurements of He-, Ar-, and N_2-broadened HF lineshapes in the first overtone band," *J. Mol. Spectrosc.* **196**, 70–76 (1999).
74. R. Meredith, "Strengths and widths in the first overtone band of hydrogen fluoride," *J. Quant. Spectrosc. Radiat. Transf.* **12**, 485–492 (1972).
75. S.-I. Chou, D. Baer, and R. Hanson, "Spectral intensity and lineshape measurements in the first overtone band of HF using tunable diode lasers," *J. Mol. Spectrosc.* **195**, 123–131 (1999).
76. https://hitran.org
77. R. Kochanov et al, "HITRAN Application Programming Interface (HAPI): a comprehensive approach to working with spectroscopic data," *J. Quant. Spectrosc. Radiat. Transf.* **177**, 15–30 (2016).
78. L. Régalia et al., "Laboratory measurements and calculations of line shape parameters of the H_2O–CO_2 collision system," *J. Quant. Spectrosc. Radiat. Transf.* **231**, 126–135 (2019).
79. R. R. Gamache, M. Farese, and C. L. Renaud, "A spectral line list for water isotopologues in the 1100-4100 cm^{-1} region for application to CO_2-rich planetary atmospheres," *J. Mol. Spectrosc.* **326**, 144–150 (2016).
80. N. N. Lavrentieva and A. S. Dudaryonok, "OCS-CO_2 line broadening coefficients and their temperature dependences for the Earth and Venus atmospheres," *Icarus* **336**, 113452 (2020).
81. J. S. Wilzewski et al., "H_2, He, and CO_2 line-broadening coefficients, pressure shifts and temperature-dependence exponents for the HITRAN database. Part 1: SO_2, NH_3, HF, HCl, OCS and C_2H_2," *J. Quant. Spectrosc. Radiat. Transf.* **168**, 193–206 (2016).
82. E. Ducreux et al., "Measurements of H_2O broadened by CO_2 line-shape parameters: beyond the Voigt profile," *J. Quant. Spectrosc. Radiat. Transf.* **323**, 109026 (2024).
83. V. Devi et al., "Line parameters for CO_2 broadening in the v_2 band of $HD^{16}O$," *J. Quant. Spectrosc. Radiat. Transf.* **187**, 472–488 (2017).
84. A. Fedorova et al., "New 1.38-μm water vapor band spectroscopy for a CO_2 atmosphere: H_2O measurements in the Martian atmosphere in the SPICAM/MEX and ACS NIR/TGO experiments," *Cosmic Res.* **62**, S1–S11 (2024).
85. E. Ducreux, "On the impact of using air-collisional parameters for H_2O retrievals in CO_2-rich atmospheres," *J. Quant. Spectrosc. Radiat. Transf.* (in prep.) (2025).
86. L. Rothman et al., "HITEMP, the high-temperature molecular spectroscopic database," *J. Quant. Spectrosc. Radiat. Transf.* **111**(15), 2139–2150 (2010).
87. I. E. Gordon, L. S. Rothman, and G. C. Toon, "Revision of spectral parameters for the B- and γ-bands of oxygen and their validation against atmospheric spectra," *J. Quant. Spectrosc. Radiat. Transf.* **112**, 2310–2322 (2011).
88. G. C. Toon et al., "HITRAN spectroscopy evaluation using solar occultation FTIR spectra," *J. Quant. Spectrosc. Radiat. Transf.* **182**, 324–336 (2016).
89. K. S. Olsen et al., "Validation of the HITRAN 2016 and GEISA 2015 line lists using ACE-FTS solar occultation observations," *J. Quant. Spectrosc. Radiat. Transf.* **236**, 106590 (2019).
90. P. Connes et al., "Traces of HCl and HF in the atmosphere of Venus," *Astrophys. J.* **147**, 1230–1237 (1967).
91. G. Keating et al., "Models of Venus neutral upper atmosphere: structure and composition," *Adv. Space Res.* **5**, 117–171 (1985).
92. B. Bézard et al., "The deep atmosphere of Venus revealed by high-resolution nightside spectra," *Nature* **345**, 508–511 (1990).
93. J. B. Pollack et al., "Near-infrared light from Venus' nightside—a spectroscopic analysis," *Icarus* **103**, 1–42 (1993).
94. E. Marcq et al., "Composition and chemistry of the neutral atmosphere of Venus," *Space Sci. Rev.* **214**, 10 (2018).
95. L. V. Zasova et al., "Structure of the Venusian atmosphere from surface up to 100 km," *Cosmic Res.* **44**, 364–383 (2006).
96. J.-L. Bertaux et al., "VEGA 1 and VEGA 2 entry probes: an investigation of local UV absorption (220-400 nm) in the atmosphere of Venus (SO_2 aerosols, cloud structure)," *J. Geophys. Res. Planets* **101**(E5), 12709–12745 (1996).
97. V. A. Krasnopolsky, "A sensitive search for nitric oxide in the lower atmospheres of Venus and Mars: detection on Venus and upper limit for Mars," *Icarus* **182**(1), 80–91 (2006).
98. J.-M. Hartmann, C. Boulet, and D. Robert, *Collisional Effects on Molecular Spectra*, 2nd ed., Elsevier (2021).

99. B. Bézard et al., "The 1.10- and 1.18-μm nightside windows of Venus observed by SPICAV-IR aboard Venus Express," *Icarus* **216**(1), 173–183 (2011).
100. B. Bézard et al., "Water vapor abundance near the surface of Venus from Venus Express/VIRTIS observations," *J. Geophys. Res. Planets* **114**(E5), E00B39 (2009).
101. R. Haus and G. Arnold, "Radiative transfer in the atmosphere of Venus and applications to surface emissivity retrieval from VIRTIS/VEX measurements," *Planet. Space Sci.* **58**, 1578–1598 (2010).
102. D. Kappel et al., "Refinements in the data analysis of VIRTIS-M-IR Venus nightside spectra," *Adv. Space Res.* **50**(2), 228–255 (2012).
103. L. V. Zasova et al., "Structure of the Venus atmosphere," *Planet. Space Sci.* **55**, 1712–1728 (2007).
104. M. Sneep and W. Ubachs, "Direct measurement of the Rayleigh scattering cross section in various gases," *J. Quant. Spectrosc. Radiat. Transf.* **92**, 293–310 (2005).
105. J. B. Pollack, "Distribution and source of the UV absorption in Venus' atmosphere," *J. Geophys. Res.* **85**, A13–8141 (1980).
106. K. F. Palmer and D. Williams, "Optical constants of sulfuric acid; application to the clouds of Venus?," *Appl. Opt.* **14**, 208–219 (1975).
107. D. Nevejans et al., "Compact high-resolution spaceborne echelle grating spectrometer with acousto-optical tunable filter based order sorting for the infrared domain from 2.2 to 4.3 μm," *Appl. Opt.* **45**, 5191–5206 (2006).
108. E. Neefs et al., "NOMAD spectrometer on the ExoMars trace gas orbiter mission: part 1—design, manufacturing and testing of the infrared channels," *Appl. Opt.* **54**, 8494–8520 (2015).
109. A. C. Vandaele et al., "NOMAD, an integrated suite of three spectrometers for the ExoMars Trace Gas Mission: technical description, science objectives and expected performance," *Space Sci. Rev.* **214**, 80 (2018).
110. R. De Cock et al., "Design of the VenSpec-H instrument on ESA's EnVision mission: development of critical elements, highlighting the FFCP and grating," *Proc. SPIE* **13144**, 131440E (2024).
111. N. Mueller, S. Smrekar, and C. Tsang, "Multispectral surface emissivity from VIRTIS on Venus Express," *Icarus* **335**, 113400 (2020).
112. J. T. Erwin, in prep. (2025).

Séverine Robert, after her PhD in sciences (ULB, Belgium), joined the Planetary Atmospheres Group at the Royal Belgian Institute for Space Aeronomy (BIRA-IASB) as an expert in molecular spectroscopy. First on the SOIR's dataset and then on NOMAD's, she acquired expertise in retrieval methods and also in instrumental and mission development. She is currently an instrument lead scientist of VenSpec-H and head of the "Planetary Atmospheres" research unit and of the "Solar Radiation in Atmospheres" scientific division.

Biographies of the other authors are not available.